Assessment of Current Density Singularity in Electromigration of Solder Bumps

Pridhvi Dandu and Xuejun Fan
Department of Mechanical Engineering
Lamar University
PO Box 10028, Beaumont, TX 77710, USA
Tel: 409-880-7792; xuejun.fan@lamar.edu

Abstract

This paper investigates the current density singularity in electromigration of solder bumps. A theoretical analysis is performed on a homogenous wedge with arbitrary apex angle, $2(\pi - \theta_0)$, when the current flow passes through. A potential difference is applied at a distance far away from the tip of the wedge. It is found that current density singularity exists at the tip of the wedges when the angles $\theta_0 < 90^\circ$. The acute angles represent the corner configuration of the actual solder bump and the interconnect. The current crowding in bumps is a result of singularity exhibited at such corners. Finite element results confirm that the maximum current density has strong dependence on mesh size. To eliminate the singularity effect, a volume-averaged current density approach, over a crescent shape where the maximum current density occurs, is suggested. Such an averaged value represents the concentration of current flow in the region, and is also insensitive to mesh sizes over a large range of crescent thickness.

Introduction

Electromigration (EM) in solder bumps is a failure mechanism due to the mass transport of metal atoms when there is moment transfer between the conducting electrons (current flow) and diffusing metal ions. This generates voids on the cathode side and hillocks on the anode side of the solder bump. In the early days of the discovery of EM in interconnects, such as Al, Fiks [1] and Huntington et al. [2] proved electron wind force to be a major contribution to EM. Later Black has developed an equation relating the mean time to failure (MTTF) to the current density as shown:

$$MTTF = Aj^{-n}\, exp\left(\frac{Q}{kT}\right) \quad (1)$$

where A is constant, j is current density, n is a model parameter of current density, Q is the activation energy, k is Boltzmann's constant, and T is the conductor temperature [3]. Black has provided the above equation to analyze failure in Al interconnects. When Black's equation was used to predict the MTTF of solder bumps, the numerical results varied with the experimental results [4-6]. This is because that Black's equation assumes that the current density in interconnects to be fairly uniform and constant, whereas in solder bumps current crowding occurs at the entrance of the solder bump.

A preliminary study by the authors has revealed that finite element models using a relatively fine mesh will always generate a higher value of current density. On the contrary a relatively coarse mesh will generate a lower value of current density [7]. This deviation in the output may influence the EM reliability prediction.

In this work, an analytical model is developed to find out whether the singularity of current density exists when the current passes through the solder bump and interconnect interface. Since the geometry of solder bumps and interconnect interface is very complex, a simple wedge-like shape is considered in this paper. Furthermore the material of the wedge is assumed to be homogenous and a variety of wedge shapes are tested for singularity. In addition, a volume averaging approach is proposed to obtain consistent results regardless of mesh sizes.

Study of Singularity of Current Density in Metal Conductors

The current crowding occurs in metal conductors when there is a change in the current flow direction because of a sudden change in cross-section area. This current crowding is the main cause for the EM phenomenon. In solder bumps current crowding occurs at the nearest corner from where current enters the bump. The present work is focused on solving a singular problem using an analytical model. The geometry at the intersection of the solder bump and interconnect is very complex. To simplify, a wedge-shaped geometry is considered with arbitrary apex angle, $2(\pi - \theta_0)$, as shown in Figure 1. It is assumed that the wedge is made up of homogenous material. The current flows through the wedge.

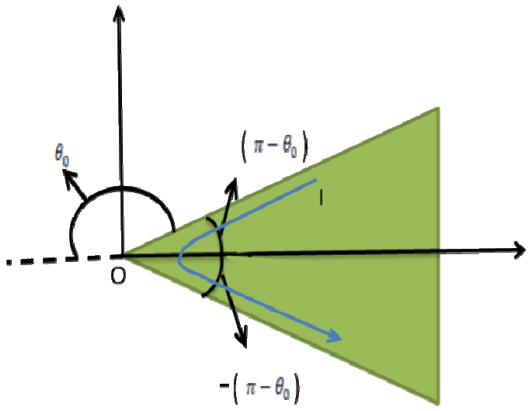

Figure 1 Current flow through a wedge of apex angle $\boldsymbol{2(\pi - \theta_0)}$

A voltage function in polar coordinates is assumed of the form

$$V(r,\theta) = r^{\lambda} f(\theta) \quad (2)$$

where λ is to be determined as part of the solution. With this choice of voltage function, the current density components in polar coordinates can be expressed as following:

$$j_r = -\frac{1}{\rho}\frac{\partial V}{\partial r} = -\frac{1}{\rho}\lambda\, r^{\lambda-1} f(\theta) \quad (3)$$

$$j_\theta = -\frac{1}{\rho}\frac{1}{r}\frac{\partial V}{\partial \theta} = -\frac{1}{\rho}\frac{1}{r}\, r^{\lambda} f'(\theta) \quad (4)$$

where ρ is resistivity of the material. The boundary conditions (BC) required on the faces of wedge are:

$$j_\theta = 0, \text{ at } \theta = \pm(\pi - \theta_0) \text{ for all r} \quad (5)$$

Substituting the BC, $j_\theta = 0$ in the Equation (4) leads to

$$\frac{\partial V}{\partial \theta} = -\frac{1}{\rho}\frac{1}{r} r^\lambda f'(\theta) = 0 \quad \text{at } \theta = \pm(\pi - \theta_0) \text{ for all r} \quad (6)$$

Since $\lambda \neq 0$, at $\theta = \pm(\pi - \theta_0)$ we have

$$f'(\theta) = 0 \quad (7)$$

From the governing equation of electrostatics, we have

$$\nabla^2 V = 0 \quad (8)$$

where $\nabla^2 = \left(\frac{\partial}{\partial r^2} + \frac{1}{r}\frac{\partial}{\partial r} + \frac{1}{r^2}\frac{\partial}{\partial \theta^2}\right)$, substituting the assumed voltage function, into the Equation (8), we get a homogeneous linear differential equation with constant coefficients as shown

$$f''(\theta) + f(\theta)\lambda^2 = 0 \quad (9)$$

The solution for $f(\theta)$, obtained by solving the above equation is

$$f(\theta) = A\cos\lambda(\theta) + B\sin\lambda(\theta) \quad (10)$$

where the constants A and B are to be determined. Applying Equation (7) to the wedge faces which are at angles $(\pi - \theta_0)$ and $-(\pi - \theta_0)$, to the general form of $f(\theta)$ in Equation (10) produces a system of two simultaneous equations with unknown constants. These equations can be represented in a matrix form as:

$$\begin{bmatrix} -\sin\lambda(\pi - \theta_0) & \cos\lambda(\pi - \theta_0) \\ \sin\lambda(\pi - \theta_0) & \cos\lambda(\pi - \theta_0) \end{bmatrix} \cdot \begin{bmatrix} A \\ B \end{bmatrix} = 0 \quad (11)$$

Since Equation (11) is homogeneous, the determinant of coefficient matrix must be equal to zero in order to get meaningful solutions. So,

$$\sin 2\lambda(\pi - \theta_0) = 0 \quad (12)$$

and, the roots of this equation are obtained as follows,

$$\lambda = \frac{n\pi}{2(\pi - \theta_0)} \quad \text{where } n = 0, \pm 1, \pm 2, \ldots \quad (13)$$

Substituting the value of λ in the voltage function, we have the general solution for a wedge with arbitrary apex angle, $2(\pi - \theta_0)$:

$$V(r,\theta) = \sum_{n=-\infty}^{\infty} r^{\left(\frac{n\pi}{2(\pi-\theta_0)}\right)} f_i(\theta) \quad (14)$$

For all values of $n < 0$, the voltage goes to infinity at the origin, which is not physically reachable. All these roots are rejected and the general solution consisting of all the acceptable terms becomes:

$$V(r,\theta) = \sum_{n=0}^{\infty} r^{\left(\frac{n\pi}{2(\pi-\theta_0)}\right)} f_i(\theta) \quad (15)$$

Expanding the above equation for all values of n:

$$V(r,\theta) = f_0(\theta) + r^{\left(\frac{\pi}{2(\pi-\theta_0)}\right)} f_1(\theta) + r^{\left(\frac{2\pi}{2(\pi-\theta_0)}\right)} f_2(\theta) + r^{\left(\frac{3\pi}{3(\pi-\theta_0)}\right)} f_3(\theta) + \cdots \quad (16)$$

For $n \geq 2$, $\frac{\partial V}{\partial r}$ equals to zero as r approaches zero (i.e. at origin). As $\frac{\partial V}{\partial r}$ is a part of current density component j_r(Equation (3)), it's logical that j_r also equal to zero at the origin. For n = 0, $\frac{\partial V}{\partial r}$ will be equal to zero. When n = 1, i.e. the second term in the expanded Equation (16), $\frac{\partial V}{\partial r}$ is:

$$\frac{\partial V}{\partial r} = \left(\frac{\pi}{2(\pi - \theta_0)}\right) \cdot r^{\left(\frac{2\theta_0 - \pi}{2(\pi - \theta_0)}\right)} f_1(\theta) \quad (17)$$

In the above equation, the exponential of 'r', i.e. $\left(\frac{2\theta_0 - \pi}{2(\pi - \theta_0)}\right)$, generates negative values for some values of θ_0. In such cases, $\frac{\partial V}{\partial r}$ approaches infinity as r approaches zero. As a result current density also approaches infinity. This shows that singularity of current density exists for some angles of θ_0. Two general cases are discussed below. Case 1 discusses about the wedge with acute angles ($\theta_0 < 90°$) and Case 2 discusses angles greater than equal to 90 ($\theta_0 \geq 90°$).

Case 1: When $\theta_0 < \frac{\pi}{2}$, $\frac{2\theta_0 - \pi}{2(\pi - \theta_0)} < 0$. Equation (17) indicates that $\frac{\partial V}{\partial r}$, or j_r becomes infinity when r approaches zero. For example when $\theta_0 = 0$, the wedge is fully closed upon itself and takes the shape of a crack as shown in Figure 2. When $\theta_0 = \frac{\pi}{4}$, wedge has a shape of V-notch as shown in Figure 3.

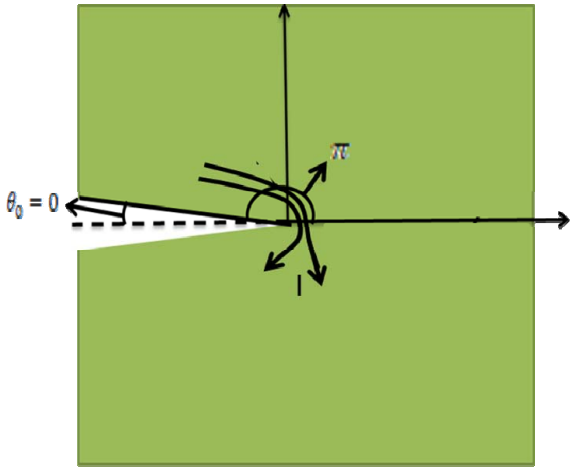

Figure 2 A wedge with an angle $\theta_0 = 0$ resembling a crack

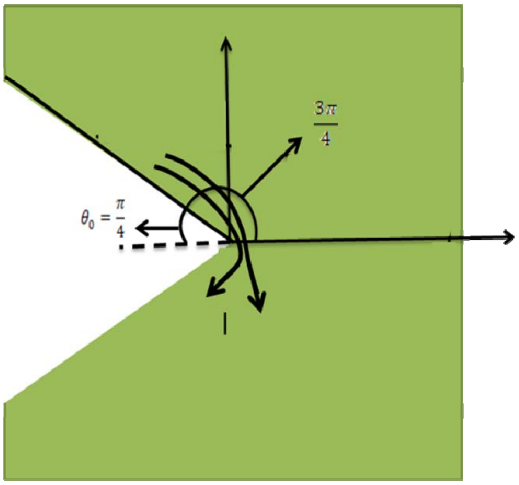

Figure 3 A wedge with an angle $\theta_0 = \frac{\pi}{4}$ resembling a V-notch

Substituting the values of θ_0 in Equation (17), we get

$$\text{For } \theta_0 = 0 \quad \frac{\partial V}{\partial r} = \frac{1}{2} r^{\frac{-1}{2}} [A\cos\frac{\pi}{2} + B\sin\frac{\pi}{2}] \quad (18)$$

For $\theta_0 = \frac{\pi}{4}$ $\quad \frac{\partial V}{\partial r} = \frac{2}{3} r^{\frac{-1}{3}} [\mathrm{A}\cos\frac{\pi}{2} + \mathrm{B}\sin\frac{\pi}{2}]$ (19)

In Equations (18) and (19) the exponential of r is negative for both the angles. When r approaches zero, $\frac{\partial V}{\partial r}$ approaches infinity. Subsequently current density also equals to infinity. This shows that the current density is unbounded and thus the singularity exist at the origin.

Case 2: $\pi \geq \theta_0 \geq \frac{\pi}{2}, \frac{2\theta_0 - \pi}{2(\pi - \theta_0)} \geq 0$. From Equation (17), the $\frac{\partial V}{\partial r}$ will not become infinity when r approaches zero. Two special cases with $\theta_0 = \frac{\pi}{2}$, and $\theta_0 = \frac{3\pi}{4}$ are shown in Figure 4 and 5 respectively. When $\theta_0 = \frac{\pi}{2}$, the wedge becomes a vertical free surface. The current flows in the direction parallel to the surface as shown in Figure 4. When $\theta_0 = \frac{3\pi}{4}$, the wedge takes the shape of a cone and the flow of the current in this case is as shown in Figure 5.

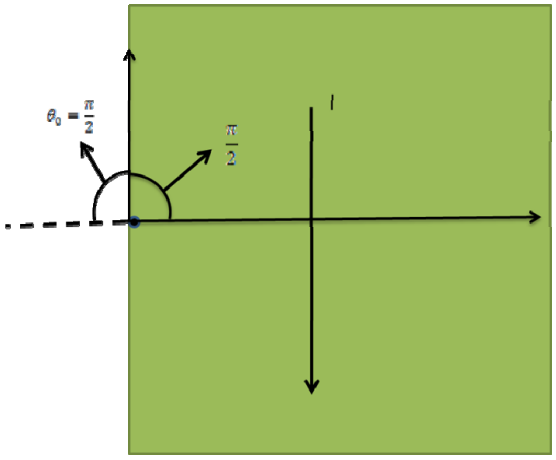

Figure 4 A wedge with an angle $\theta_0 = \frac{\pi}{2}$ resembling a vertical free surface

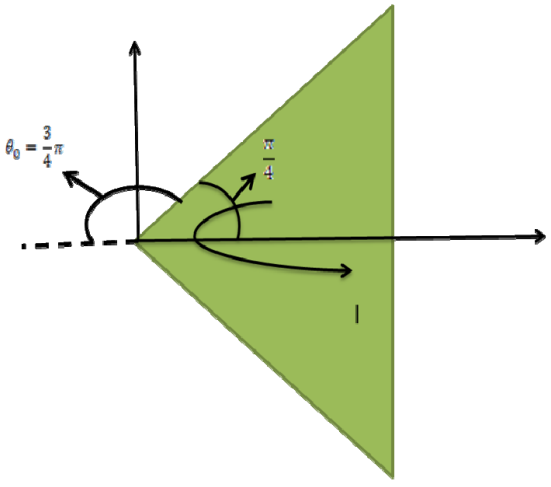

Figure 5 A wedge with an angle $\theta_0 = \frac{3}{4}\pi$ resembling a cone

Substituting the values of θ_0 in Equation (17), we get

For $\theta_0 = \frac{\pi}{2}$ $\quad \frac{\partial V}{\partial r} = r^0 [\mathrm{A}\cos\frac{\pi}{2} + \mathrm{B}\sin\frac{\pi}{2}]$ (20)

For $\theta_0 = \frac{3}{4}\pi$ $\quad \frac{\partial V}{\partial r} = 2r[\mathrm{A}\cos\frac{\pi}{2} + \mathrm{B}\sin\frac{\pi}{2}]$ (21)

In Equations (20) and (21) the exponential of r is ≥ 0 for both the angles. In both cases when r approaches zero the current density is bounded.

It can be inferred from the above study that the current density singularity arises for wedges with acute θ_0 angles ($\theta_0 < 90°$). For the wedges with angles ($\theta_0 \geq 90°$) there is no current density singularity observed. In actual solder bump geometry, where solder bump is attached to a different material (ex. copper), the singularity is expected to occur with the geometry given. This has been evident with finite element results in reference [8], and more results will be shown in next section.

Numerical Investigation and Volume Averaging

To solve the current flow problem, a finite element model as shown in Figure 6 is considered. The figure shows five solder bumps (with copper posts on top of them) electrically connected with each other in a daisy chain format. To simplify the model, only the corner bump is designed in actual ball shape and the rest of the bumps are considered as rectangular blocks. At one end of the electrical connection, the voltage potential is set grounded (zero), while at the other end a lumped current load of 1.7 Amps [9] is applied. Since the current flows from top to bottom portion of the corner bump, electromigration would occur at the bottom of the bump. Hence the focus of this work is the bottom portion of corner bump.

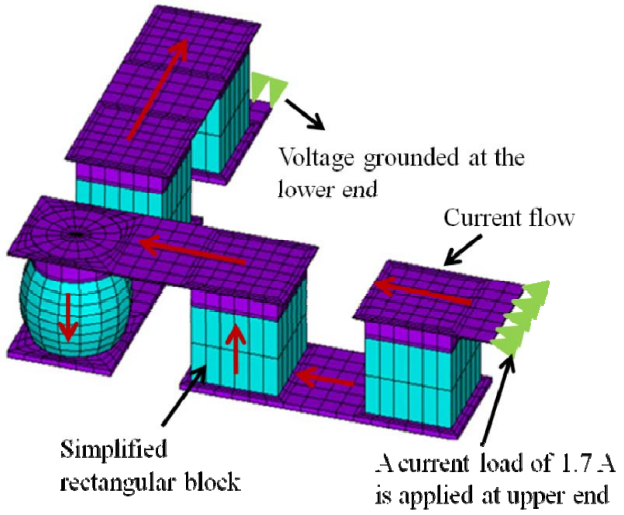

Figure 6 Finite element model with boundary conditions and current flow direction

To investigate the effects of mesh size, three different mesh schemes are considered. Figure 7 shows three mesh patterns, denoted by 'X', 'X/2' and 'X/4', indicating the mesh size is reduced by a factor of two each time. The maximum current density at the bottom of the bump will be extracted.

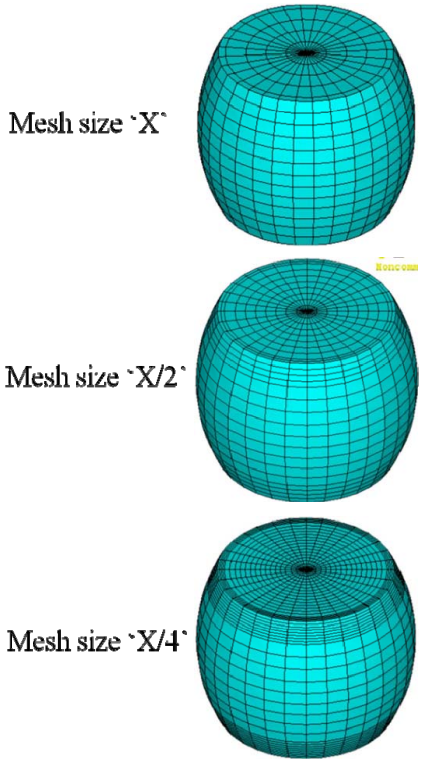

Figure 7 Three different mesh schemes

To remove the singularity effect, one method is to extract the averaged current density over certain volumes. In this method the current density is averaged over all the elements of the selected volumes as following:

$$\Delta J_{ave} = \frac{\Sigma \Delta J \cdot V_o}{\Sigma V_o} \qquad (22)$$

where, ΔJ_{ave} is average current density, ΔJ is current density in each element, V_o is volume of each element. Two different volume averaging approaches are studied. In the first approach, the current density is averaged over entire bottom surface, as shown in Figure 8. For all three different mesh sizes, the thickness of bottom disk is fixed.

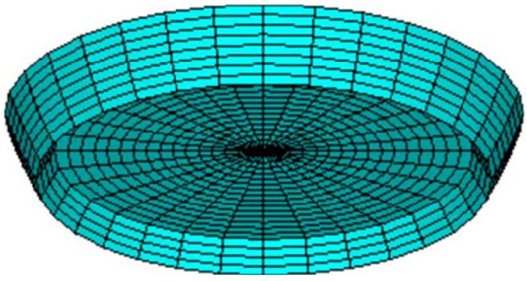

Figure 8 An entire disk volume at the bottom of solder bump for averaging

According to the conservation of current flow, the current passing through the disk will remain same if the bump shape is same. Such an averaged value may not reflect the current crowding at the entrance of the bumps. Therefore, in the second approach, a crescent shaped portion is selected from the outer most ring of the bottom disk, where maximum current density is observed. Figure 9 shows the crescent selected from the outer most ring of the bottom disk. The crescent is selected in such a way that the maximum current density location coincides with the center of it. Three different ring sizes, termed p/r ratios, as shown in Figure 10, are studied to better understand the concentration of current flow in the current crowding regions of solder bump. For each p/r ratio, three mesh sizes are applied as shown in Figure 11.

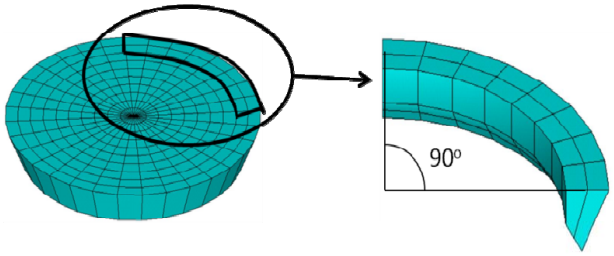

Figure 9 Crescent volume from the bottom disk volume

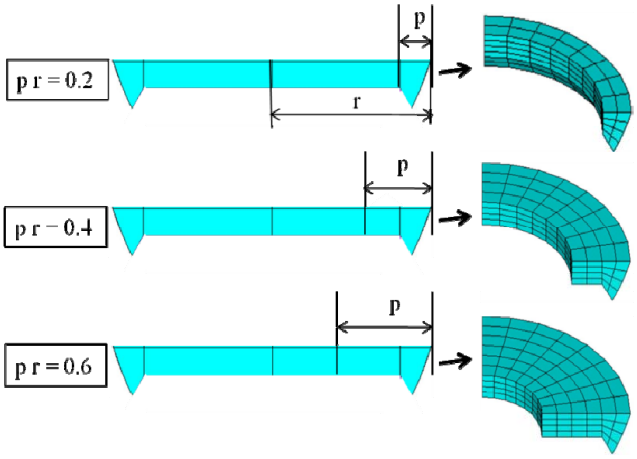

Figure 10 Crescents with three p/r ratios

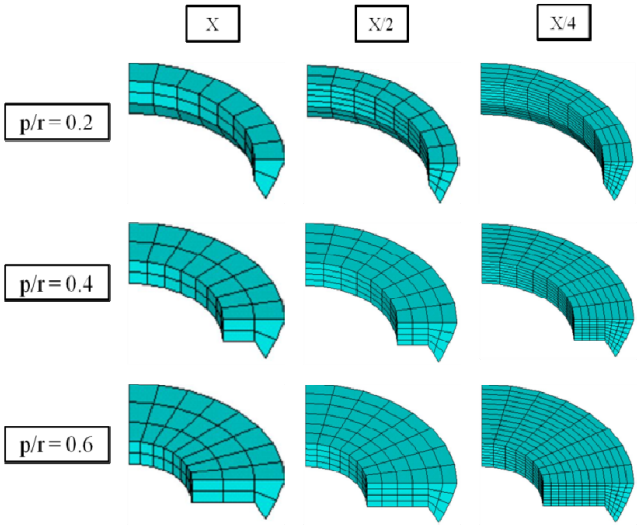

Figure 11 Crescents with three different mesh schemes

Results

Figure 12 shows the contours of the current density in bottom layer with three different meshes. Cleary it shows the strong dependency with mesh size. The values of maximum and average current densities of bottom disk with different

mesh sizes are tabulated in Table 1. As the mesh size is reduced by a factor of four, the maximum current density has increased by 24%. The average current densities calculated in the bottom disk for all the mesh schemes are the same. It is observed that the averaging has decreased the current density value in bottom disk by 56% compared to the maximum current density (in the case of 'X/4' mesh size).

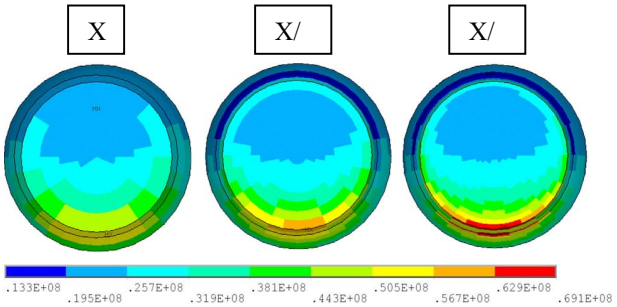

Figure 12 Current density contours with different meshes in the bottom disk

Table 1 The Maximum and Average Current Densities Calculated in Bottom Disk for Different Mesh Sizes

Mesh Size	Max. Current dens. (Bottom Disk & Crescent) (A/m^2)	Average Current dens. in Bottom Disk (A/m^2)
x	0.55e8	0.30e8
x/2	0.60e8	0.30e8
x/4	0.69e8	0.30e8

Table 2 summarizes all the averaged current density values calculated for all thicknesses (p/r = 0.2, 0.4 and 0.6) of crescents with different meshes. It can be inferred that, for a crescent size of p/r = 0.2, the average current densities calculated with all the mesh sizes are nearly same and are not mesh size dependent. A similar trend was also observed for crescent size of p/r = 0.4 and 0.6. No change in average current density is observed for crescent as the p/r value increases from 0.2 to 0.4. But when p/r is increased from 0.4 to 0.6 the average current density has decreased by a small amount.

Table 2 The Average Current Densities of all the Crescents Thicknesses with Different Mesh Sizes

Mesh Size	Average Current dens. (A/m^2) in Crescent with		
	p/r = 0.2	p/r = 0.4	p/r = 0.6
x	0.45E8	0.45e8	0.43e8
x/2	0.44E8	0.44e8	0.42e8
x/4	0.44E8	0.44e8	0.42e8

The results presented in Table 2 show that the concentration of current density is placed on a crescent region where the current flows through. Even the p/r ratio increases up to 0.6, the averaged current density remain a relatively constant value, and this value is significantly higher than the averaged value over entire disk volume (Table 1). Therefore, the averaged current density over the crescent shape can be used when predicting the reliability under current stressing.

Conclusions

In this work, a homogenous wedge with arbitrary apex angle, $2(\pi - \theta_0)$, has been used to conduct an analytical model study to examine the singularity of current density in solder bumps. Effect of wedge angles on the singularity is studied in detail. Current density singularity is only observed in wedges with acute angles $\theta_0 < 90^\circ$. Finite element modeling indicates that current density exhibits a strong mesh-size dependency, signaling the existence of singularity at the corner of solder bumps. To eliminate the singularity effect, a volume averaging method is suggested. Furthermore, a volume-averaging approach based on a crescent-shape volume, where the maximum current density occurs, is introduced. It is observed in the averaged current density is a relatively constant value over a large range of crescent thickness with different mesh sizes. Such value is significantly higher than the current density averaged over the entire bottom layer. Therefore, the averaged current density over the crescent shape can be used when predicting the reliability under current stressing.

References

1. Fiks, V.B., Mechanics of the mobility of ions in metals, Soviet Physics Solid State, v. 1, No. 1, pp. 14-28, 1959.
2. Huntington, H. B. and Grone, A. R., Current- induced marker motion in gold wires, Journal of Physics and Chemistry of Solids, v. 20, No. 1, pp. 76-87, 1961.
3. Black, J. R., Electromigration failure modes in Aluminum metallization for semiconductor devices, IEEE, v. 57, No. 9, pp. 1587-1594, 1969.
4. Tu, K.N., Recent advances on electromigration in every-large-scale-integration of interconnects, Journal of Applied Physics, v. 94, No. 9, pp. 5451-5473, 2003.
5. Liang, S.W., Shao, T.L. and Chen, C., 3-D simulation on current density distribution in flip-chip solder joints with thick Cu UBM under current stressing, Proc. of Electronic components and technology conference (ECTC), pp. 1416–1420, 2005.
6. Rinne, G., Electromigration in SnPb and Pb-free solder bumps, Proc. of Electronic components and technology conference (ECTC), pp. 974-978, 2004.
7. Dandu, P., Fan, X. J., Liu, Y. and Diao, C., Finite element modeling on electromigration of solder joints in wafer level packaging, Microelectronic Reliability, v. 50, pp. 547-555, 2010.
8. Dandu, P., Fan, X. J. and Liu, Y., Some Remarks on Finite Element Modeling of Electromigration in Solder Joints, Proc. of Electronics Components and Technology Conference (ECTC), pp. 396-402, 2010.
9. Liu, Y., Liang, L., Irving, S. and Luk, T., 3D modeling of electromigration combined with thermalmechanical effect for IC device and package, Microelectronics Reliability, v. 48, pp. 811-824, 2008.